Journal of the American Heart Association

ORIGINAL RESEARCH

Arterial Platelet Adhesion in Atherosclerosis-Prone Arteries of Obese, Insulin-Resistant Nonhuman Primates

Eran Brown, BS; Koya Ozawa (iD), MD, PhD; Federico Moccetti (iD), MD; Amanda Vinson, PhD; James Hodovan, RDCS; The Anh Nguyen, MS; Lindsay Bader, BS; José A. López, MD; Paul Kievit (iD), PhD; Gray D. Shaw, BS; Dominic W. Chung, PhD; Warren Osborn, BS; Xiaoyun Fu, PhD; Junmei Chen, PhD; Jonathan R. Lindner (iD), MD

BACKGROUND: Platelet–endothelial interactions are thought to contribute to early atherogenesis. These interactions are potentiated by oxidative stress. We used in vivo molecular imaging to test the hypothesis that platelet–endothelial interactions occur at early stages of plaque development in obese, insulin-resistant nonhuman primates, and are suppressed by NADPH-oxidase-2 inhibition.

METHODS AND RESULTS: Six adult rhesus macaques fed a Western-style diet for a median of 4.0 years were studied at baseline and after 8 weeks of therapy with the NADPH-oxidase-2-inhibitor apocynin (50 mg/kg per day). Six lean control animals were also studied. Measurements included intravenous glucose tolerance test, body composition by dual-energy X-ray absorptiometry, carotid intimal medial thickness, carotid artery contrast ultrasound molecular imaging for platelet GPIbα (glycoprotein-Ibα) and vascular cell adhesion molecule-1, and blood oxidative markers on mass spectrometry. Compared with lean controls, animals on a Western-style diet were obese (median body mass: 16.0 versus 8.7 kg, $P=0.003$; median truncal fat: 49% versus 20%, $P=0.002$), were insulin resistant (4-fold higher insulin–glucose area under the curve on intravenous glucose tolerance test, $P=0.002$), had 40% larger carotid intimal medial thickness ($P=0.004$), and exhibited oxidative signatures on proteomics. In obese but not lean animals, signal enhancement on molecular imaging was significantly elevated for GPIbα and vascular cell adhesion molecule-1. The signal correlated modestly with intimal medial thickness but not with the degree of insulin resistance. Apocynin significantly ($P<0.01$) reduced median signal for GPIbα by >80% and vascular cell adhesion molecule-1 signal by 75%, but did not affect intimal medial thickness, body mass, or intravenous glucose tolerance test results.

CONCLUSION: In nonhuman primates, diet-induced obesity and insulin resistance leads to platelet–endothelial adhesion at early atherosclerotic lesion sites, which is associated with the expression of pro-inflammatory adhesion molecules. These responses appear to be mediated, in part, through oxidative pathways.

Key Words: atherosclerosis ■ molecular imaging ■ platelets ■ von Willebrand factor

Platelet–endothelial interactions are thought to contribute to early atherogenesis.[1,2] In preclinical models of atherosclerosis, platelet adhesion is mediated largely through interactions with endothelial-associated von Willebrand factor (VWF) in lesion-prone arterial regions.[3–6] Adherent platelets potentially accelerate atherosclerosis by recruiting leukocytes, serving as a source for pro-inflammatory cytokines and inflammasome activation, and suppressing inflammation resolution.[1,7–10] Most data implicating platelet–endothelial interactions in atherogenesis have come primarily from rabbit and transgenic murine models of

JAHA is available at: www.ahajournals.org/journal/jaha

CLINICAL PERSPECTIVE

What Is New?

- In obese and insulin-resistant primates that closely mimic the human condition, platelet adhesion directly to the endothelium of atherosclerosis-prone arterial sites can be observed before any meaningful plaque occurs.
- Platelet adhesion is associated with pro-inflammatory endothelial activation, and occurs in conjunction with increased blood markers of increased oxidative stress.
- Novel antioxidant compounds, such as the plant-derived acetovanillone apocynin, reduces oxidative stress, platelet adhesion, and endothelial activation.

What Are the Clinical Implications?

- Platelet–endothelial interactions could represent a novel therapeutic target for mitigating the increased risk for atherosclerosis in obesity and insulin resistance.
- Naturally occurring NADPH inhibitors represent a new approach for ameliorating the pro-atherosclerotic effects of diet-related obesity.

Nonstandard Abbreviations and Acronyms

ADAMTS-13	a disintegrin and metalloproteinase with a thrombospondin type-1 motif member 13
CEU	contrast-enhanced ultrasound
DEXA	dual-energy X-ray absorptiometry
NOX2	NADPH-oxidase-2
ROS	reactive oxygen species
VCAM-1	vascular cell adhesion molecule-1
VWF	von Willebrand factor
WSD	Western-style diet

hyperlipidemia, and from in vitro experiments where human platelets were co-incubated with vascular endothelial cells.

Obesity and insulin resistance (IR) are risk factors for atherosclerosis involving vascular endothelial and platelet activation.[11–13] The overlapping factors that contribute to activation include oxidative stress, increased cytokine production, and toxic effects of glycation and free fatty acids.[12–14] Oxidative modification in particular increases endothelial-associated ultralarge VWF multimers through transcriptional regulation, mobilization of endothelial Weibel-Palade bodies, and reduction in the ability of ADAMTS13 (a disintegrin and metalloproteinase with a thrombospondin type-1 motif member 13) to proteolytically cleave VWF multimers.[15–18] Whether obesity and IR also increase platelet adhesion at atherosclerosis-prone sites is unknown. In this study, we used molecular imaging in rhesus macaques to test whether platelet–endothelial interactions occur in primates with diet-induced obesity, and whether they are associated with the degree of IR, or with other markers of endothelial activation. Because of the putative role of reactive oxygen species (ROS) in promoting an increase in endothelial-associated ultralarge VWF,[17,18] we also investigated whether platelet adhesion occurs in concert with markers of increased oxidative stress in blood, and whether platelet adhesion could be suppressed by apocynin, an acetovanillone that has several antioxidant properties including inhibition of endothelial NADPH-oxidase-2 (NOX2), and has been demonstrated to reduce platelet–endothelial interactions and progression of atherosclerosis in hyperlipidemic mice.[19,20]

METHODS

Study Design

The data that support the findings of this study are available from the corresponding author upon reasonable request. The study was approved by the Animal Care and Use Committee of the Oregon National Primate Research Center at Oregon Health & Science University and was performed in accordance with the guidelines of the United States Department of Agriculture and Association for Assessment and Accreditation of Laboratory Animal Care concerning handling of nonhuman primates. We studied adult male rhesus macaques (*Macaca mulatta*) ages 6 to 18 years (n=6) fed a Western-style diet (WSD) (caloric content: 18.4% protein, 36.6% fat, and 45.0% carbohydrates, with 612 ppm cholesterol) for 2 to 6 years in order to produce obesity and IR of various degrees. Obese animals were studied at baseline and after 8 weeks of therapy with oral apocynin (50 mg/kg per day). Age-matched control macaques (n=6) on chow diet (14.7% calories from fat with 27 ppm cholesterol) were also studied once. Each study was performed over 3 days and included the following: (1) dual x-ray absorptiometry (DEXA) assessment of central adiposity, (2) intravenous glucose tolerance test, (3) carotid ultrasound imaging for plaque and intima-medial dimension, (4) carotid contrast-enhanced ultrasound (CEU) molecular imaging for platelet GPIbα (glycoprotein-Ibα) and vascular cell adhesion molecule-1 (VCAM-1), (5) assessment of vascular mechanical properties by pulse-wave velocity, (6) coronary microvascular flow reserve by vasodilator stress myocardial contrast echocardiography perfusion imaging, and (7) analysis by mass spectrometry for markers of oxidative stress. Anesthesia was induced with ketamine (10 mg/kg IM) and maintained with isoflurane

(1.0%–1.5%) except for DEXA and intravenous glucose tolerance test procedures for which telazol (5 mg/kg IM) was used. At the completion of the 8-week therapy, apocynin therapy was stopped and animals were returned to the obese resource of the Oregon National Primate Research Center.

Intravenous Glucose Tolerance Test

Animals were fasted overnight and sedated. After DEXA scanning, dextrose (600 mg/kg) was administered intravenously. Venous blood samples were collected before injection and after 1, 3, 5, 10, 20, 40, and 60 minutes. Concentrations of blood glucose (Onetouch Ultra Glucose monitor, LifeScan) and plasma insulin (Roche Diagnostics Cobas e411, Indianapolis, IN) were measured and plotted as time–concentration curves. Results were reported as the product of the areas under the curve of glucose and insulin, and as the basal homeostatic model assessment for insulin resistance index, calculated as follows: homeostatic model assessment for insulin resistance = [fasting insulin (µIU/mL) × fasting glucose (mmol/L)]/22.5.

Body Composition

Body composition was assessed by performing DEXA (Discovery A, Hologic Inc). Visceral adiposity was calculated by dividing truncal fat mass by total truncal mass.

Molecular Imaging Agent Preparation

Biotinylated, lipid-shelled decafluorobutane microbubbles were prepared by sonication of a gas-saturated aqueous suspension of distearoylphosphatidylcholine (2 mg/mL), polyoxyethylene-40-stearate (1 mg/mL), and distearoylphosphatidylethanolamine-PEG (2000) biotin (0.4 mg/mL). Microbubbles were targeted to VCAM-1 and platelet GPIbα as previously described,[5] via surface conjugation of mouse anti-human monoclonal IgG1 against VCAM-1 (1.G11B1), or a 15-amino acid cyclic peptide (CCP-015b) biotinylated at an added C-terminal lysine residue and based on the previously reported synthetic OS-1 peptide that binds with high affinity to primate GPIbα (Quell Pharma Inc., Plymouth, MA).[21] Unconjugated microbubbles with no targeting ligand were used as controls. Microbubble concentration was measured by electrozone sensing (Multisizer III, Beckman-Coulter).

Validation of Platelet-Targeted Contrast Agent

Because CEU molecular imaging in nonhuman primates (NHPs) has been established for VCAM-1 but not platelet GPIbα,[22] an in vitro flow chamber assay was used to assess attachment of GPIbα-targeted MBs to rhesus macaque platelets. Collagen-coated culture dishes were blocked with human serum albumin (2.5%) and mounted on a rectangular flow chamber. Platelet-rich plasma from WSD–fed rhesus macaques was placed on the dishes for 10 minutes and washed with PBS. Suspensions of GPIbα-targeted and control MBs ($5×10^6$ mL^{-1} in PBS) differentially labeled with the lipophilic fluorophores and dioctadecyl tetramethylindocarbocyanine perchlorate and dioctadecyloxacarbocyannine perchlorate, respectively, were drawn through the chamber at a shear stress of 1.0, 2.0, or 8.0 dyne/cm^2 for 5 minutes. Plates were washed for 5 minutes with PBS at the same shear rates after which microbubble attachment to adherent platelets was assessed by fluorescent microscopy in 10 randomly selected nonoverlapping optical fields (0.03 mm^2). Data were expressed as a ratio of fluorescent microbubbles area to platelet area, and were separately analyzed for regions with (1) single platelets or aggregates <50 µm^2, or (2) platelet aggregates >50 µm^2, because of the tendency of the latter to produce regional variations in shear.

CEU Molecular Imaging

Bilateral ultrasound molecular imaging of the distal common carotid artery and bulb was performed in long-axis using multipulse contrast-specific imaging at 7 MHz, a mechanical index of 1.9, a dynamic range of 55 dB, and a frame rate of 1 Hz (Sequoia, Siemens Medical Imaging, Mountain View, CA). Intravenous injections of $1×10^8$ targeted microbubbles agents were performed in random order. After each injection, ultrasound was paused for 1 minute, after which 2-dimensional ultrasound at low power (mechanical index <0.10) was used to locate the carotid artery before activating contrast-specific imaging for several frames. To minimize signal from freely circulating agent, the left ventricle of the heart was simultaneously (at 1 minute postinjection) exposed to high mechanical index (1.3) ultrasound at 1.3 MHz and a frame rate of 25–30 Hz. Signal for retained agent in each carotid artery was quantified by digitally averaging the first 2 frames acquired and subtracting several averaged frames acquired after >5 destructive pulse sequences. Signals from regions-of-interest at the near and far walls of the distal common and proximal internal carotid artery were averaged.

Carotid Morphometry and Vascular Stiffness

The carotid artery was imaged in long axis by 2-dimensional ultrasound using a linear array probe at 18 MHz (Logiq E9; GE Healthcare, Waukesha, WI). Common carotid intimal medial thickness (IMT) was expressed as the average of ≥3 far-wall measurements. Carotid plaque was defined by focal thickening

of >1 mm or the presence of calcification. Pulse-wave velocity, an index of vascular stiffness, was assessed by spectral pulse-wave Doppler measurement of the time delay of the onset of systolic forward velocity between the aortic arch and femoral artery, using the ECG as a time reference, divided by the distance between them. Data were averaged for 3 cardiac cycles.

Myocardial Perfusion Imaging

Transthoracic myocardial contrast echocardiography was performed with a phased-array probe (Sonos 5500; Philips Ultrasound, Andover, MA). Myocardial contrast echocardiography was performed using power modulation imaging at 1.6 MHz and a mechanical index of 0.18 during an intravenous infusion of lipid-shelled decafluorobutane microbubbles (1×10^8 min^{-1}). End-systolic images were acquired after a high-power (mechanical index 1.0) destructive pulse sequence. Imaging was performed in the apical 4- and 2-chamber views at rest and during adenosine stress (140 mg/kg per minute). Postdestructive time-intensity data from 2 separate coronary artery territories were fit to the function:

$$y = A\left(1 - e^{-\beta t}\right) \quad\quad (1)$$

where y is intensity at time t, A is plateau intensity representing relative microvascular blood volume, β is the microvascular flux rate, and the product of A and β is an index of myocardial blood flow.

Plasma Lipid, Cytokine, and VWF Measurement

Cytokine levels from venous blood samples were determined using a monkey multiplex cytokine panel (ThermoFisher Scientific, Waltham, MA) following the manufacturer's instructions. Samples were analyzed on a Milliplex Analyzer (EMD Millipore, Billerica, MA) bead sorter with XPonent Software version 3.1 (Luminex, Austin, TX). Data were calculated using Milliplex Analyst software version 5.1 (EMD Millipore). Intra-assay CVs for all analytes were <15%. Citrated venous blood samples were used to quantify circulating VWF concentration via sandwich ELISA.[23]

Flow Cytometry

Flow cytometry of platelet-rich plasma stored in sodium citrate was performed for surface markers of platelet activation, including CD41 and p-selectin (Data S1).

Blood Oxidative Markers

Markers of oxidative stress in citrated whole blood were measured by mass spectrometry. These measurements included total thiol and glutathione concentration, and

the proportion of each that was in the reduced state, and the presence of mixed disulfides such as cysteine-glycine (Cys-Gly), which have been recently identified as a plasma biomarker of oxidative stress.[24] Full descriptions of methods are provided in Data S1.

Statistical Analysis

Data were analyzed on Prism v.8.0. Depending on whether data were normally or nonnormally distributed (based on the D'Agostino and Pearson omnibus test), differences between cohorts were assessed by a 1-way ANOVA or Kruskal–Wallis test with Dunn's multiple comparison. Post hoc testing was performed with a Mann Whitney U test or, for differences between baseline and postapocynin conditions, a Wilcoxon rank sum test. Correlations were made using linear regression and a Spearman rho test. Comparisons were considered significant at $P<0.05$.

RESULTS

Body Morphometry, Metabolic Status, and Plasma Lipids

For animals on WSD, the median duration on the diet was 4.0 years (interquartile range [IQR]: 3.5–4.6 years). Compared with lean controls, animals on WSD before treatment with apocynin (baseline) had greater body mass and truncal adiposity on DEXA (Figure 1A and 1B). The insulin and glucose areas under the curve product on intravenous glucose tolerance test and homeostatic model assessment for insulin resistance index showed variable degrees of IR in the obese animals on WSD (Figure 1C and 1D). Obese animals also had significantly elevated baseline plasma total cholesterol, LDL-C (low-density lipoprotein cholesterol), and triglycerides (Figure 1E through 1H). Treatment of obese animals with 8 weeks of apocynin did not significantly alter the body mass, truncal fat, degree of IR, or lipid status.

Blood Markers of Oxidative Stress

On evaluation of thiol species in whole blood and plasma, glutathione was by far the most abundant thiol, accounting for >85% of thiols. When compared with lean controls, obese animals on WSD had decreased amounts of reduced blood thiols, which was attributable to a decrease in reduced glutathione in whole blood (Figure 2A through 2F). In plasma, cysteine and Cys-Gly were the main thiols while protein-bound cysteine and Cys-Gly were the most abundant protein disulfide–bound adducts (Figure S1), all of which have been associated with increased oxidative stress.[24] Total cysteine and protein-bound cysteine tended to be higher in obese animals (Figures 2G and 2H), though these differences did not reach statistical significance. However, total Cys-Gly
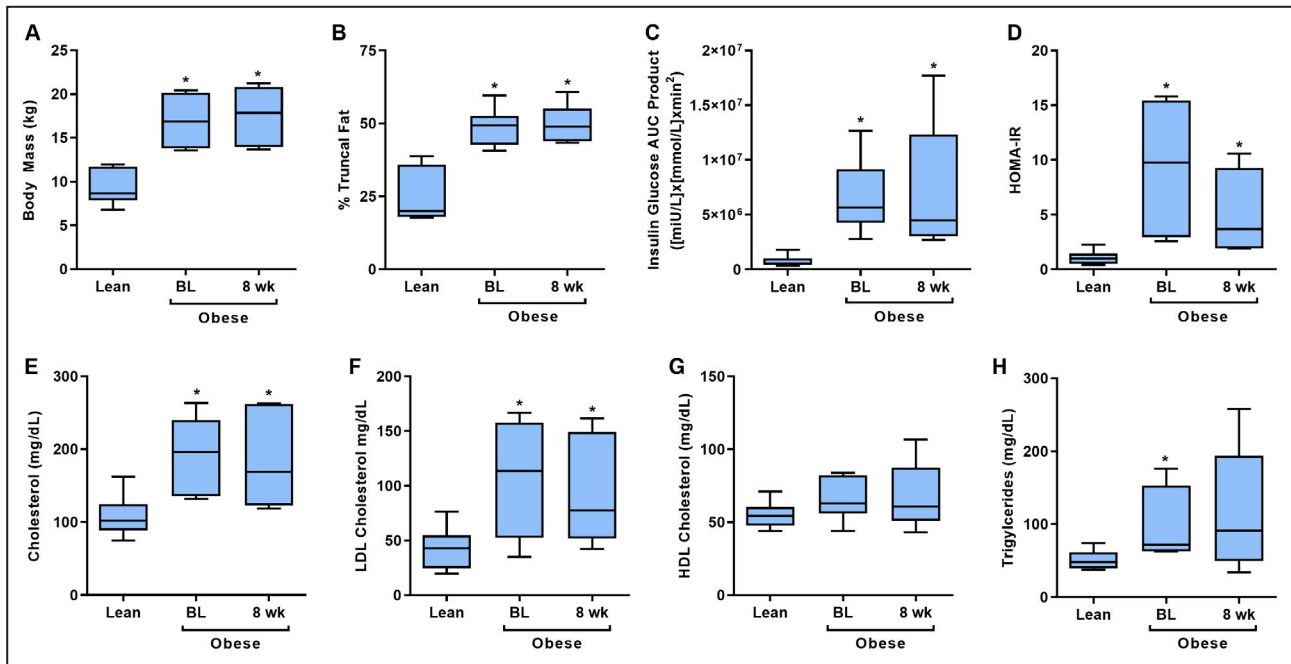
Figure 1. Indices of metabolic status in lean rhesus macaques, and obese animals on WSD at BL and after 8 weeks of apocynin treatment.

Bar-whisker plots illustrate the median (bar), interquartile range (box), and range (whiskers) for (**A**) body mass, (**B**) truncal fat on DEXA, (**C**) product of insulin and glucose AUC on IVGTT, (**D**) HOMA-IR index, (**E**) serum cholesterol, (**F**) LDL cholesterol, (**G**) HDL cholesterol, and (**H**) serum triglycerides. *$P<0.05$ vs lean. AUC indicates area-under-the-curve; BL, baseline; DEXA, dual-energy x-ray absorptiometry; HDL, high-density lipoprotein; HOMA-IR, homeostatic model assessment for insulin resistance; IVGTT, intravenous glucose tolerance test; LDL, low-density lipoprotein; and WSD, Western-style diet.

and protein-bound Cys-Gly were significantly higher in the obese animals (Figures 2I and 2J). Plasma concentrations of 8-series F_2-isoprostane were also higher in obese animals (Figure 2K). Cumulatively, these results indicate greater oxidative stress in NHPs on WSD. Statistical power for detecting changes in oxidative stress after apocynin treatment was limited by hemolysis in several samples. Yet apocynin treatment resulted in significant increases in reduced thiols (median 0.50 [IQR, 0.46–0.54] versus 0.56 [IQR, 0.53–0.59], $P=0.03$) and reduced glutathione (median 0.49 [IQR, 0.45–0.52] versus 0.55 [IQR, 0.52–0.58], $P=0.03$).

Vascular Morphology and Function

There were no significant groupwise or stagewise differences in heart rate, nor systolic or diastolic blood pressure (Table S1). Carotid IMT was greater in obese animals on WSD than in lean controls (Figure 3). Three obese animals had evidence of mild discrete plaque in 1 common or external carotid artery. There were no groupwise differences in aortic stiffness on pulse-wave velocity. In obese animals, neither carotid IMT nor pulse-wave velocity was significantly changed by 8 weeks of apocynin treatment.

Myocardial contrast echocardiography perfusion imaging at rest and during adenosine was performed

to assess coronary microvascular response, abnormalities of which are often associated with impaired endothelial function and oxidative stress. A significant groupwise difference was found for microvascular flux rate (β-value) during adenosine stress (Table 1). Although post hoc analysis between groups for all measurements did not reach statistical significance after correcting for multiple comparisons, there were consistent trends towards lower resting and hyperemic values for microvascular flux rate (β-value), blood flow, β-reserve, and flow reserve in obese animals versus lean controls. Treatment of obese animals with apocynin also tended to produce higher hyperemic microvascular flux rate and perfusion, and greater β-reserve and flow reserve. Vital signs at rest and during stress were similar between groups (Table S1).

Carotid Molecular Imaging

In vitro flow chamber studies were used to assess binding of GPIbα-targeted microbubbles to platelets from rhesus macaques. Platelet-targeted microbubbles selectively attached to single platelets and platelet aggregates, whereas attachment for nontargeted control agent was rare (Figure 4A and 4B). Shear-dependent attachment was observed for attachment to single platelets or small platelet aggregates. Shear
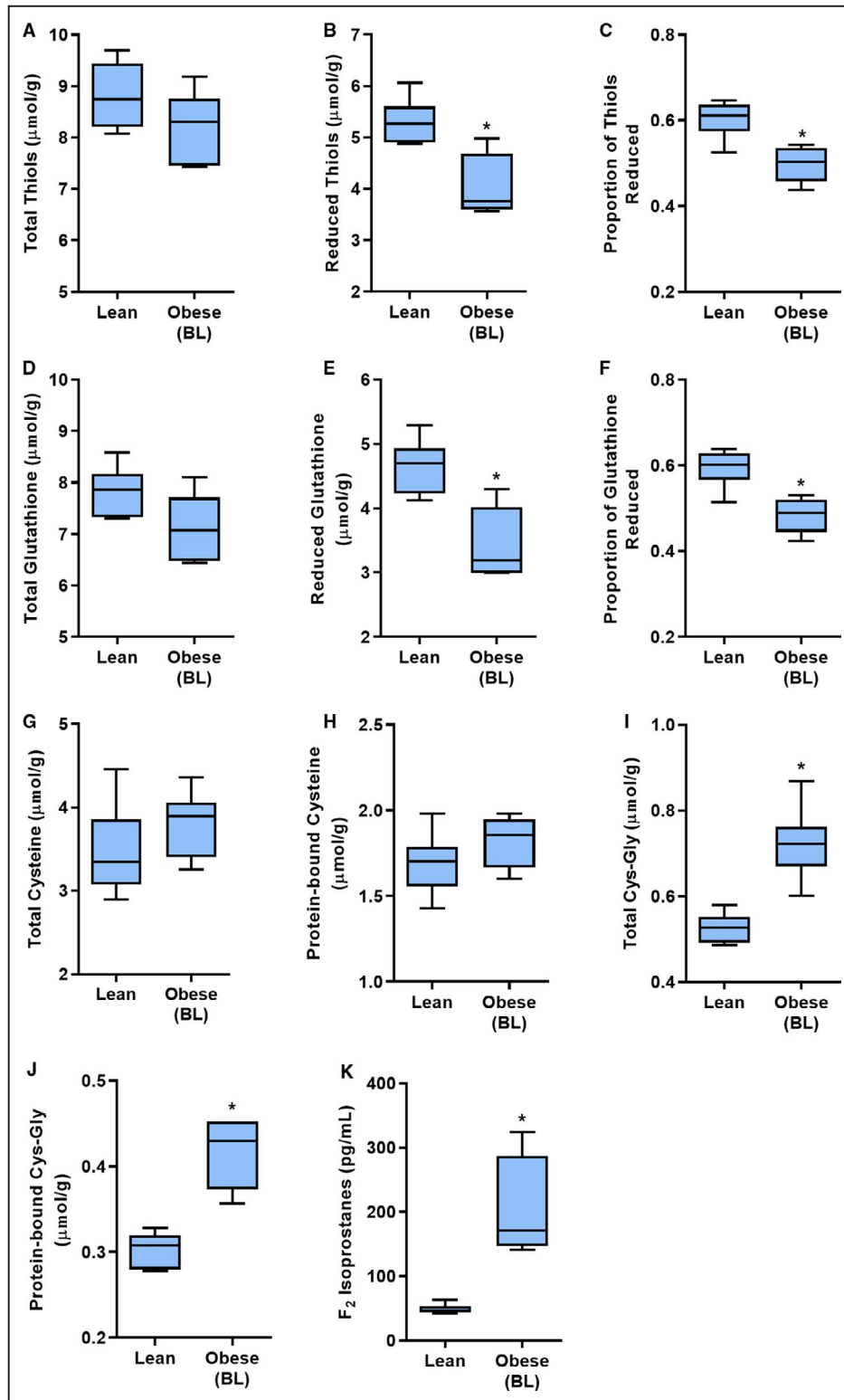
Figure 2. Blood markers of oxidative stress in lean animals and in obese animals at BL study.
The markers include: (**A**) total thiol concentration in whole blood, (**B**) reduced thiols, (**C**) proportion of thiols in a reduced state, (**D**) total glutathione concentration normalized to hemoglobin, (**E**) reduced glutathione, and (**F**) proportion of glutathione in a reduced state. The thiol concentrations in panels A to F were normalized to hemoglobin concentration. Plasma markers included: (**G**) total cysteine in plasma, (**H**) protein-bound cysteine, (**I**) total Cys-Gly in plasma, (**J**) protein-bound Cys-Gly, and (**K**) plasma F_2-isoprostane concentrations by ELISA. The thiol concentrations in panels G to J were normalized to total protein concentration. *$P<0.05$ vs lean controls. BL indicates baseline.
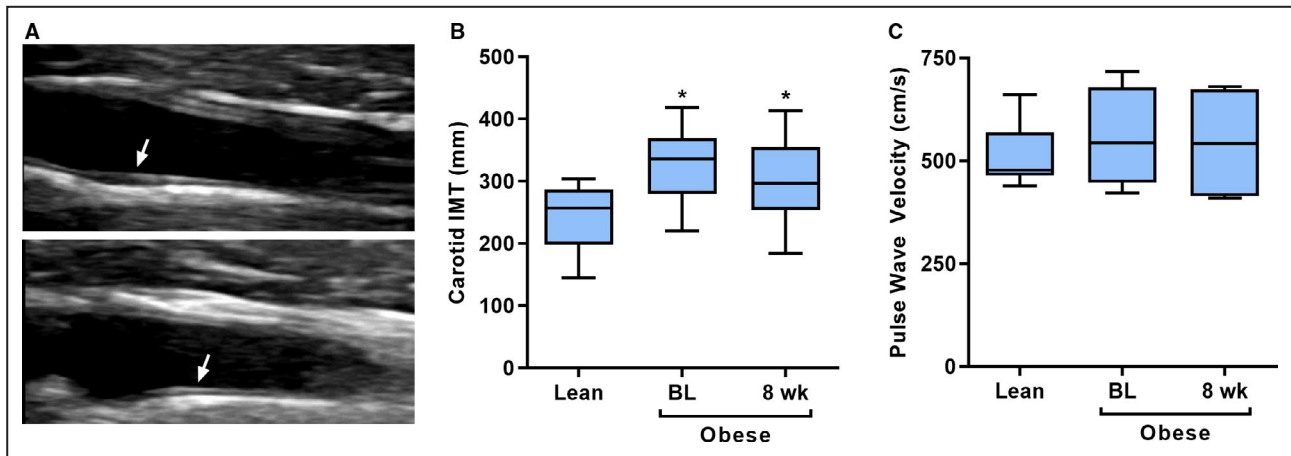
Figure 3. Vascular morphology and functional analysis in lean rhesus macaques, and obese animals on WSD at BL and after 8 weeks of apocynin treatment.
A, Example of IMT thickening in the carotid bulb (arrow, top) and common carotid artery (arrow, bottom). Bar-whisker plots illustrate the median (bar), interquartile range (box), and range (whiskers) for (**B**) carotid IMT, and (**C**) pulse wave velocity. *P<0.05 vs lean. BL indicates baseline; IMT, intima-medial thickness; and WSD, Western-style diet.

dependency was not found for large aggregates, likely because of the potential of large aggregates to interrupt laminar flow and create regions of shear heterogeneity along the aggregate surface.

CEU molecular imaging of the carotid arteries for platelet GPIbα at the endothelial surface and for endothelial VCAM-1, a marker of inflammatory activation, revealed low signal enhancement in lean control animals similar to that generated from control contrast agent (Figure 4C). In animals on WSD, signal for both VCAM-1 and platelet GPIbα was elevated compared with nontargeted agent, and higher than that from lean control animals. Signal for platelet GPIbα modestly correlated with that from VCAM-1 within the same carotid arteries (Figure 4D). There was no morphologic evidence for carotid thrombus formation at the sites

of platelet molecular imaging signal. Neither platelet GPIbα nor VCAM-1 signal on CEU was found to correlate with body mass, truncal adiposity, time on WSD, or degree of IR on intravenous glucose tolerance test (Table 2), although a modest but significant relationship was found between GPIbα signal and body mass and adiposity. Carotid IMT was found to correlate modestly with signal for both platelet GPIbα and VCAM-1 signal (Table 2, Figure S2). Flow cytometry for platelet markers of inflammation, including CD41 and p-selectin, indicated that apocynin had no effect on platelet activation status, although there also was no evidence for increased platelet activation in the obese versus lean animals (Figure S3).

In obese animals, 8 weeks of therapy with apocynin significantly reduced the carotid molecular imaging

Table 1. Rest and Vasodilator Stress Myocardial Perfusion Values Derived From MCE*

		Obese (n=6)	
	Lean (n=6)	Baseline	8 Wks Apocynin
Rest			
Flux rate (β-value, s⁻¹)	1.1 (0.74–1.37)	0.68 (0.37–1.13)	0.61 (0.48–1.10)
MBF (Aβ, IU/s)	110 (61–150)	66 (32–119)	51 (39–84)
Vasodilator stress			
Flux rate (β-value, s⁻¹)	1.72 (1.51–2.43)	1.04 (0.76–1.32)†	1.48 (0.86–2.33)
MBF (Aβ, IU/s)	168 (122–270)	97 (64–127)†	168 (122–270)
Reserve (stress/rest)			
β-reserve	1.72 (1.41–2.53)	1.17 (1.05–2.33)	1.61 (1.37–3.96)
MBF reserve	1.70 (1.12–2.61)	1.43 (1.03–2.25)	1.81 (1.44–3.96)

MBF indicates myocardial blood flow; and MCE, myocardial contrast echocardiography.
*Data are display as median (interquartile range).
†P<0.05 versus lean.
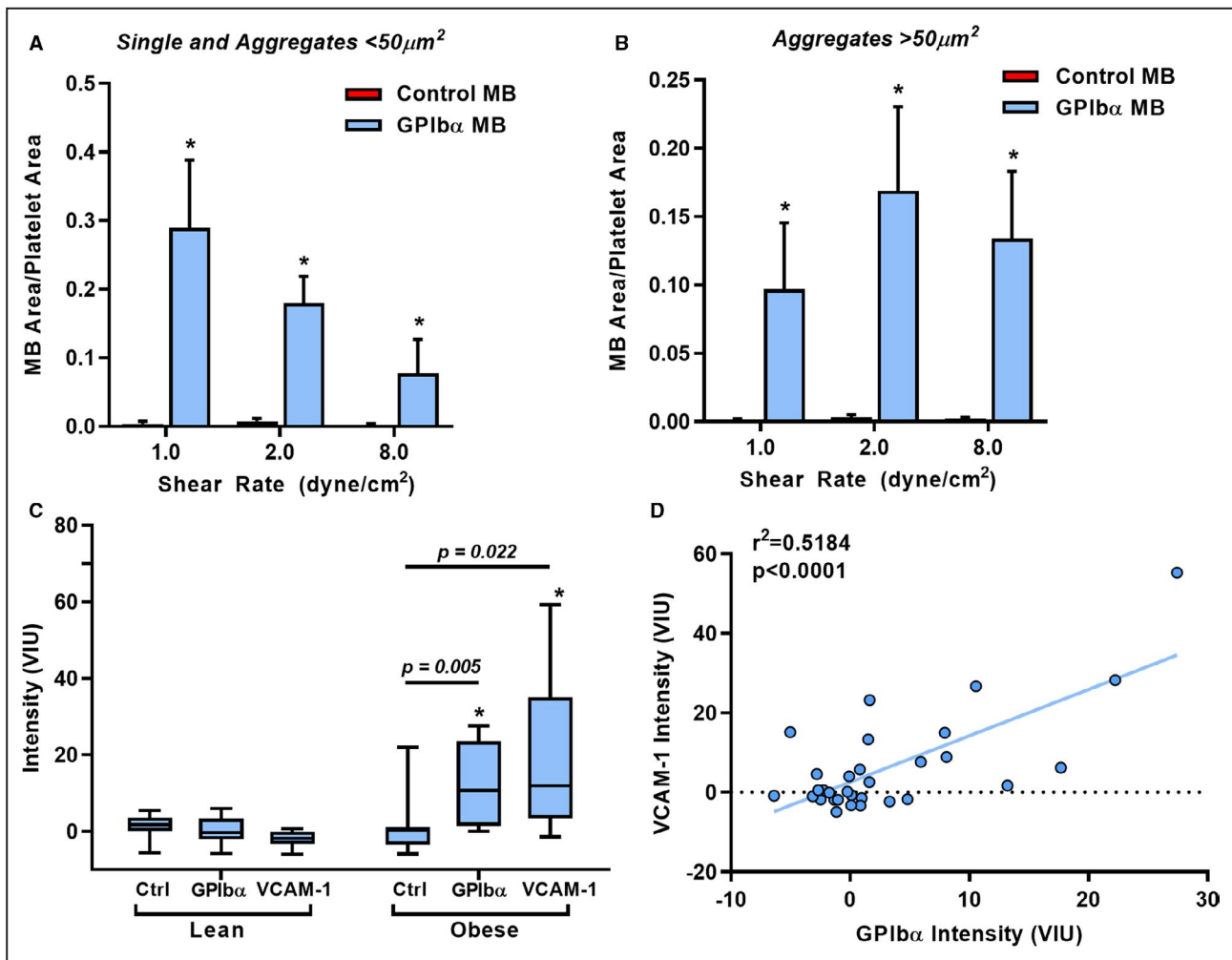
Figure 4.   In vitro flow chamber data (shear rates of 1.0–8.0 dyne/cm^2) for attachment of control and GPIbα-targeted MB for (A) single platelets and small platelet aggregates (<50 μm^2), and for (B) large platelet aggregates (>50 μm^2).
Data are quantified as mean (±SEM) fluorescent area normalized to platelet area *$P<0.05$ vs control MB. **C**, Bar-whisker plots illustrating the median (bar), interquartile range (box), and range (whiskers) for CEU molecular imaging for control (Ctrl) and targeted MB agents in lean and obese animals. *$P<0.05$ vs lean. **D**, Correlation between VCAM-1 and GPIbα signal on CEU molecular imaging on a per-artery basis. CEU indicates; GPIbα, glycoprotein Ibα; MB, microbubbles; VCAM-1, vascular cell adhesion molecule-1; and VIU, video intensity units.

signal for platelet GPIbα and VCAM-1, whereas no significant change was observed for control agent signal (Figure 5). Arteries with the highest GPIbα or VCAM-1 signal at baseline had the greatest relative decrease in signal after therapy.

In a limited array of plasma cytokines that could be measured in NHP plasma (Figure 6), compared with lean animals, obese animals at baseline had higher concentrations of higher interleukin-1 receptor antagonist (IL1-RA) and chemokine c-c motif ligand-2 (also known as monocyte chemoattractant protein-1), although statistical significance was reached only for IL1-RA and not chemokine c-c motif ligand-2. In obese animals, apocynin resulted in a decrease in interleukin-1 receptor antagonist levels, although

statistical significance was borderline. Plasma VWF antigen levels were higher in obese versus lean animals, but did not significantly change with apocynin treatment. These data indicate that groupwise differences in endothelial phenotypes on molecular imaging were associated with modest groupwise differences in circulating pro-inflammatory cytokine levels.

DISCUSSION

The critical role platelets play in acute atherothrombotic events in patients with late-stage atherosclerotic disease is well established. It is increasingly recognized that platelet adhesion promotes atherosclerotic plaque

Table 2. Correlation of Morphometric and Metabolic Data With Molecular Imaging

	GPIbα Signal (n=21)		VCAM-1 Signal (n=19)	
	Pearson *r*	*P* Value	Pearson *r*	*P* Value
Body mass	0.50	0.02	0.25	0.29
Truncal adiposity	0.55	<0.01	0.33	0.16
Time on WSD*	0.42	0.22	0.50	0.14
IVGTT AUC Product	0.40	0.07	0.39	0.09
Carotid IMT	0.54	0.01	0.59	<0.01

AUC indicates insulin-glucose area-under-the-curve; GPIbα, glycoprotein Ibα; IMT, intima-medial thickness; IVGTT, intravenous glucose tolerance test; VCAM1, vascular cell adhesion molecule-1; and WSD, Western-style diet.

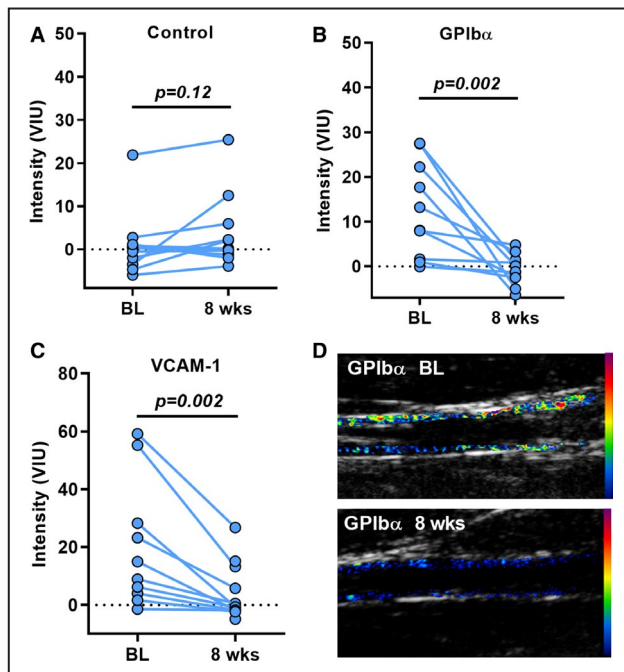*Analysis performed for obese animals only (n=12 comparisons). Pearson *r* represents the Pearson correlation coefficient.

development at an early stage through multiple pathways.[1,2,10,25] An important component of "thromboinflammation" in plaque development is the ability of platelets to influence the local balance of pro-inflammatory cytokines, ROS, and inflammasome activation status. An obstacle to studying pro-atherogenic effects of platelets is the lack of methods for assessing adhesion in vivo

Figure 5. Individual data for CEU molecular imaging signal in obese animals at BL and after 8 weeks of apocynin therapy for (A) control MB, (B) GPIbα-targeted MB, and (C) VCAM-1-targeted MB.
D, Example carotid artery CEU molecular imaging of platelet GPIbα from an obese animal at BL and after apocynin therapy. Images show background-subtracted and color-coded (scale at right) CEU signal superimposed on a co-registered 2-dimensional B-mode image. BL indicates baseline; CEU; GPIbα, glycoprotein Ibα; MB, microbubbles; VCAM-1, vascular cell adhesion molecule-1; and VIU, video intensity units.

in animal models that closely resemble humans. In this study, noninvasive ultrasound molecular imaging with targeted probes that are confined to the vascular compartment was used to examine carotid endothelial–platelet adhesion in NHPs with diet-induced obesity and IR. Our results indicate that (1) platelet adhesion occurs in atherosclerosis-prone arteries of obese rhesus macaques before significant plaque development; (2) the degree of platelet adhesion is independent of the degree of IR or obesity; (3) there is an association between the degree of platelet adhesion and other markers of endothelial activation such as VCAM-1 expression; and (4) inhibition of NOX2 with apocynin reduces both platelet adhesion and VCAM-1 expression without major changes in metabolic function or plasma cytokine levels.
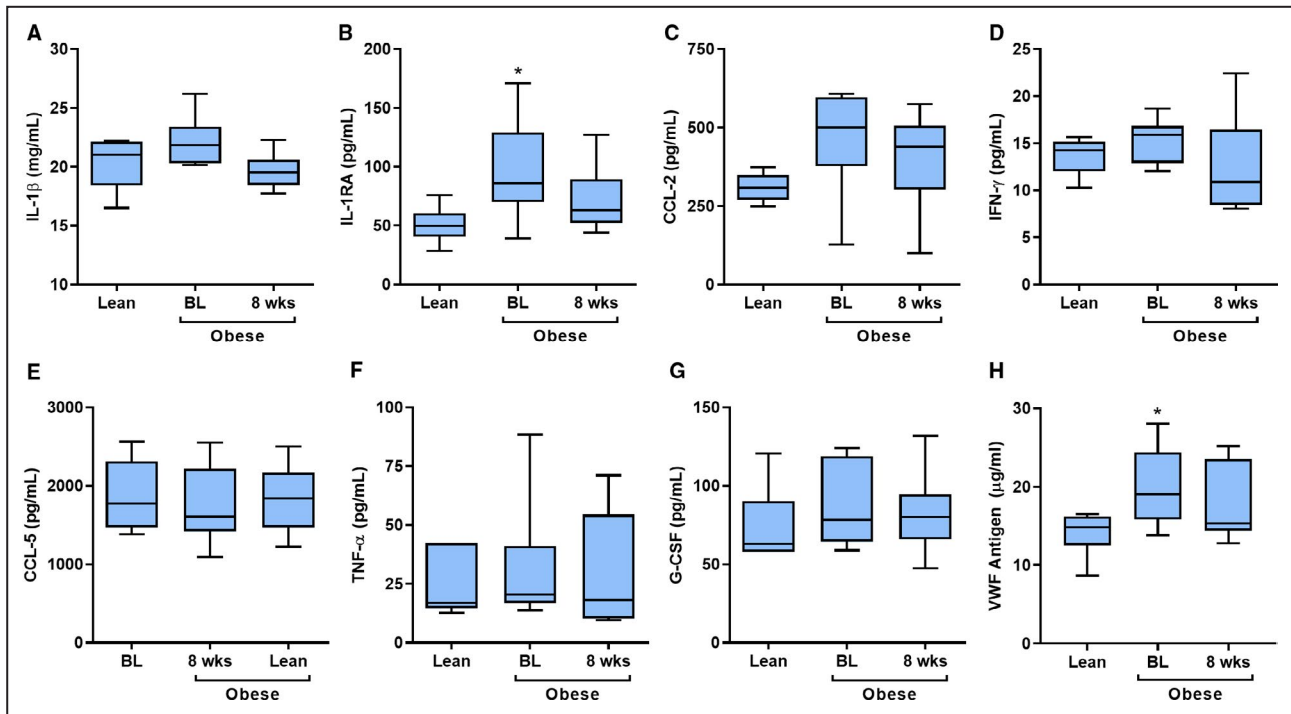
Atherosclerosis is a disease that, in most individuals, becomes clinically evident decades after disease initiation. Important insights into the pathobiology of plaque progression have been provided through gene-modified mice. Yet, our understanding of human atherosclerosis must also rely on models in which the temporal course, spatial distribution, and biologic pathways are similar to those in humans. We used an NHP model in which adult rhesus macaques were fed a diet moderately high in saturated fat and cholesterol for an average of 4 years in order to study vascular changes that occur as a result of obesity and IR. Similar to what occurs in humans, the severity of IR and lipid derangement varied substantially between individual animals. Despite the wide variation in metabolic response that occurs with this model,[26] in vivo imaging has previously demonstrated a relatively uniform time-dependent increase in endothelial VCAM-1, endothelial selectin expression, and IMT for 2 years after starting WSD.[22] These data indicate that endothelial inflammatory responses are influenced by diet-induced obesity, but are not tightly coupled to the degree of IR. Neither platelet–endothelial interactions nor the oxidative pathways that can promote these interactions have been studied previously in human or NHPs.

Platelet–endothelial interactions, primarily through interaction of GPIbα and endothelial-associated VWF, have been shown in small animal models to promote atherogenesis.[3–6] Characterization of these interactions in humanlike models of obesity and IR is important to study for several reasons. Increased oxidative stress and certain lipid derangements associated with metabolic disease are known to interfere with ADAMTS13-mediated cleavage of endothelial VWF.[17,18,23] In small clinical trials of patients with diabetes mellitus, low ADAMTS13 activity has been associated with increased rates of cardiovascular events.[27] Yet plasma levels of VWF are higher in patients with diabetes mellitus or high-risk metabolic syndrome,[28,29] and are known to progressively increase after initiating WSD in NHPs.[22] In aggregate, these data suggest that IR may be associated with increased endothelial VWF production or mobilization, and reduced

Figure 6. Bar-whisker plots illustrate the median (bar), interquartile range (box), and range (whiskers) for plasma (A) IL-1β, (B) IL-1RA, (C) CCL-2, (D) IFN-γ, (E) CCL-5, (F) TNF-α, (G) G-CSF, and (H) VWF antigen.
*P<0.05 vs lean. BL indicates baseline; CCL-2, chemokine c-c motif ligand-2; CCL-5, chemokine c-c motif ligand-5; G-CSF, granulocyte colony-stimulating factor; IFN-γ, interferon gamma; IL-1β, interleukin-1β; IL-1RA, ingterleukin-1 receptor antagonist; TNF-α, tumor necrosis factor-α; and VWF, von Willebrand factor.

ability to proteolytically cleave endothelial-associated ultralarge VWF multimers.

For the current study, platelet adhesion was imaged by using targeted microbubbles that are similar to platelets in size and that bear the 15-amino acid cyclic peptide that binds to constitutively expressed platelet GPIbα in primates.[21] A PEGylated monomeric version of this peptide has been shown to be effective in humans by inhibiting neutrophil–platelet aggregation mediated by GPIbα interaction with Mac-1.[30] CEU signal from the platelet-targeted agent in the carotid artery was significantly increased in NHPs that had diet-induced obesity, IR, and dyslipidemia. These obese animals also had evidence of early atherosclerotic changes in the form of increased IMT on carotid ultrasound, and evidence for endothelial dysfunction on coronary microvascular vasodilator testing. Carotid platelet adhesion on CEU did not correlate closely with the degree of obesity or IR, indicating that simply the presence and not the degree of metabolic derangement determines platelet adhesion. In vitro studies have indicated that platelets can activate the endothelium through platelet-derived growth factors, chemokines, and ROS.[25] Accordingly, CEU was used to also assess endothelial VCAM-1 expression, which correlated with the degree of platelet signal. The idea that platelet adhesion has a role in stimulating VCAM-1 expression is supported by studies in atherosclerotic mice where endothelial expression of VCAM-1 is influenced by manipulation of ADAMTS13 activity and GPIbα-mediated platelet adhesion.[31]

The generation of ROS is likely a common pathway linking endothelial dysfunction, VWF-mediated platelet adhesion, and diet-induced obesity or IR. Oxidative pathways are enhanced in patients with diabetes mellitus,[12] including oxidative modification of VWF.[32] In our studies, decreased levels of reduced thiols in whole blood, and increased levels of protein-bound cysteine, Cys-Gly, and F_2-isoprostanes in plasma indicated elevated oxidative stress in animals on WSD. The effects of apocynin, a plant-derived α-methoxyphenol that inhibits cytosolic assembly of NOX2 subunits,[19] were investigated based on several lines of reasoning. Murine studies have revealed a critical role of the NOX2 isoform in atherosclerosis.[33] Moreover, apocynin has been shown to reverse oxidative endothelial abnormalities attributable to hyperglycemia.[34] In several murine models of atherosclerosis, long-term therapy with apocynin has been shown to reduce endothelial platelet adhesion in mice.[6,20] This finding is congruent with the notion that ROS can stimulate endothelial secretion of VWF,[16] and render VWF less susceptible to proteolysis.[17] Flow data

indicated that platelet activation status did not play a major role in the differences in platelet adhesion seen according to cohort and treatment. This finding is aligned with human studies that have found no evidence for platelet activation from obesity alone.[35] The reduction in platelet adhesion by apocynin in murine atherosclerotic models was associated with not only reduced platelet adhesion, but also slower plaque growth, less endothelial cell adhesion molecule expression, and suppression of plaque macrophage accumulation.[6,20]

In the current study, apocynin was found to reduce carotid artery CEU signal for platelet GPIbα and VCAM-1, and to improve microvascular function in general in obese animals. This effect was independent of any major changes in the degree of obesity, IR, or lipid status. We have not yet determined whether apocynin reduced platelet adhesion by decreasing endothelial surface mobilization of ultralarge VWF multimers, by enhancing ADAMTS13-mediated cleavage of VWF, or by some other mechanism. Molecular imaging for VWF was not performed because of lack of validated probes. Molecular imaging studies performed in hyperlipidemic mice with accelerated atherosclerosis have revealed that apocynin not only reduces plaque formation as mentioned above, but reduces the endothelial VWF, and specifically the A1 binding domain for GPIbα.[6] Not included in this study were our unsuccessful attempts to measure plasma ADAMTS13 activity using assays that are linear over a wide range of activity.[36] It has been firmly established that ADAMTS13 from macaques and humans have similar proteolytic activity against human VWF.[37,38] Yet, our results indicated very low plasma ADAMTS13 activity for both obese and lean NHPs (10%–40% of human), raising concerns that our assays were adversely affected by storage, presence of citrate, and repetitive freeze–thaw cycles.

There are several important limitations of this study. The sample size was small based on the resources needed to study NHP models of sustained IR induced by WSD for several years. The extensive profiling of these animals allowed us to derive as much information as possible from this valuable and limited resource. While CEU molecular imaging provides an in vivo assessment of endothelial phenotype, histologic validation of the technique has been performed in mice, not primates. Instead, we relied on flow chamber assays for ex vivo validation of microbubbles adhesion in shear. We are, however, reassured by previous studies showing time-dependent increase in CEU signal for endothelial inflammatory activation after starting WSD,[22] and by our current findings that CEU signal correlated with carotid IMT. The premise for this study is that platelets contribute to vascular inflammatory activation

at an early stage of disease. While our study is the first to show platelet adhesion in a primate model of obesity and IR, we did not conclusively demonstrate a causative relationship between platelet adhesion, VCAM-1, and IMT. When considering the role of oxidative stress, we were not powered to determine the quantitative relationship between ROS generation and platelet adhesion. On the basis of the size of the cohort, we did not compare effects of apocynin to conventional antiplatelet agents. Because GPIbα is constitutively expressed and does not require activation, drugs such as aspirin have minimal influence on platelet adhesion to VWF or collagen.[39] Hence, while aspirin or dual antiplatelet therapy reduce aggregation and likelihood for acute thrombotic complications, they may not be entirely useful for the indolent pro-inflammatory effects of platelet adhesion.

In summary, our findings indicate that platelet–endothelial interactions occur in a NHP model of diet-induced obesity and IR at early stages of atherosclerotic intimal-medial thickening in the carotid artery. The degree of platelet adhesion correlates with the degree of VCAM-1 expression, supporting but not proving the hypothesis that platelet adhesion contributes to endothelial inflammatory activation. Treatment of animals with the NOX2-inhibitor apocynin significantly reduced carotid platelet adhesion and VCAM-1 expression without altering metabolic status. Whether this approach can suppress plaque formation will require studies with longer duration of therapy. Based on our results, further investigation of strategies to reduce platelet–endothelial interaction is warranted.

Supplementary Material
Data S1
Table S1
Figure S1–S3

REFERENCES

1. Wu MD, Atkinson TM, Lindner JR. Platelets and von willebrand factor in atherogenesis. *Blood*. 2017;129:1415–1419. DOI: 10.1182/blood-2016-07-692673.

2. Nording HM, Seizer P, Langer HF. Platelets in inflammation and atherogenesis. *Front Immunol*. 2015;6:98. DOI: 10.3389/fimmu.2015.00098.

3. Theilmeier G, Michiels C, Spaepen E, Vreys I, Collen D, Vermylen J, Hoylaerts MF. Endothelial von willebrand factor recruits platelets to atherosclerosis-prone sites in response to hypercholesterolemia. *Blood*. 2002;99:4486–4493. DOI: 10.1182/blood.V99.12.4486.

4. Massberg S, Brand K, Grüner S, Page S, Müller E, Müller I, Bergmeier W, Richter T, Lorenz M, Konrad I, et al. A critical role of platelet adhesion in the initiation of atherosclerotic lesion formation. *J Exp Med*. 2002;196:887–896. DOI: 10.1084/jem.20012044.

5. Shim CY, Liu YN, Atkinson T, Xie A, Foster T, Davidson BP, Treible M, Qi Y, López JA, Munday A, et al. Molecular imaging of platelet-endothelial interactions and endothelial von willebrand factor in early and mid-stage atherosclerosis. *Circ Cardiovasc Imaging*. 2015;8:e002765. DOI: 10.1161/CIRCIMAGING.114.002765.

6. Moccetti F, Brown E, Xie A, Packwood W, Qi Y, Ruggeri Z, Shentu W, Chen J, Lopez JA, Lindner JR. Myocardial infarction produces sustained proinflammatory endothelial activation in remote arteries. *J Am Coll Cardiol*. 2018;72:1015–1026. DOI: 10.1016/j.jacc.2018.06.044.

7. Weyrich AS, Lindemann S, Zimmerman GA. The evolving role of platelets in inflammation. *J Thromb Haemost*. 2003;1:1897–1905. DOI: 10.1046/j.1538-7836.2003.00304.x.

8. Barrett TJ, Schlegel M, Zhou F, Gorenchtein M, Bolstorff J, Moore KJ, Fisher EA, Berger JS. Platelet regulation of myeloid suppressor of cytokine signaling 3 accelerates atherosclerosis. *Sci Transl Med*. 2019;11:517. DOI:10.1126/scitranslmed.aax0481.

9. Gerdes N, Seijkens T, Lievens D, Kuijpers MJE, Winkels H, Projahn D, Hartwig H, Beckers L, Megens RTA, Boon L, et al. Platelet CD40 exacerbates atherosclerosis by transcellular activation of endothelial cells and leukocytes. *Arterioscler Thromb Vasc Biol*. 2016;36:482–490. DOI: 10.1161/ATVBAHA.115.307074.

10. Rolfes V, Ribeiro LS, Hawwari I, Böttcher L, Rosero N, Maasewerd S, Santos MLS, Próchnicki T, Silva CMdS, Wanderley CWdS, et al. Platelets fuel the inflammasome activation of innate immune cells. *Cell Rep*. 2020;31:107615. DOI: 10.1016/j.celrep.2020.107615.

11. Santilli F, Vazzana N, Liani R, Guagnano MT, Davi G. Platelet activation in obesity and metabolic syndrome. *Obes Rev*. 2012;13:27–42. DOI: 10.1111/j.1467-789X.2011.00930.x.

12. Vazzana N, Ranalli P, Cuccurullo C, Davi G. Diabetes mellitus and thrombosis. *Thromb Res*. 2012;129:371–377. DOI: 10.1016/j.thromres.2011.11.052.

13. Ormazabal V, Nair S, Elfeky O, Aguayo C, Salomon C, Zuniga FA. Association between insulin resistance and the development of cardiovascular disease. *Cardiovasc Diabetol*. 2018;17:122. DOI: 10.1186/s12933-018-0762-4.

14. Schleicher E, Friess U. Oxidative stress, age, and atherosclerosis. *Kidney Int Suppl*. 2007;72:S17–S26. DOI: 10.1038/sj.ki.5002382.

15. Xiang Y, Hwa J. Regulation of VWF expression, and secretion in health and disease. *Curr Opin Hematol*. 2016;23:288–293. DOI: 10.1097/MOH.0000000000000230.

16. Vischer UM, Jornot L, Wollheim CB, Theler JM. Reactive oxygen intermediates induce regulated secretion of von willebrand factor from cultured human vascular endothelial cells. *Blood*. 1995;85:3164–3172. DOI: 10.1182/blood.V85.11.3164.bloodjournal85113164.

17. Chen J, Fu X, Wang Y, Ling M, McMullen B, Kulman J, Chung DW, Lopez JA. Oxidative modification of von Willebrand factor by neutrophil oxidants inhibits its cleavage by ADAMTS13. *Blood*. 2010;115:706–712. DOI: 10.1182/blood-2009-03-213967.

18. Wang Y, Chen J, Ling M, Lopez JA, Chung DW, Fu X. Hypochlorous acid generated by neutrophils inactivates ADAMTS13: an oxidative mechanism for regulating ADAMTS13 proteolytic activity during inflammation. *J Biol Chem*. 2015;290:1422–1431. DOI: 10.1074/jbc.M114.599084.

19. Yu J, Weiwer M, Linhardt RJ, Dordick JS. The role of the methoxyphenol apocynin, a vascular nadph oxidase inhibitor, as a chemopreventative agent in the potential treatment of cardiovascular diseases. *Curr Vasc Pharmacol*. 2008;6:204–217. DOI: 10.2174/157016108784911984.

20. Liu Y, Davidson BP, Yue QI, Belcik T, Xie A, Inaba Y, McCarty OJT, Tormoen GW, Zhao Y, Ruggeri ZM, et al. Molecular imaging of inflammation and platelet adhesion in advanced atherosclerosis effects of antioxidant therapy with NADPH oxidase inhibition. *Circ Cardiovasc Imaging*. 2013;6:74–82. DOI: 10.1161/CIRCIMAGING.112.975193.

21. Benard SA, Smith TM, Cunningham K, Jacob J, DeSilva T, Lin L, Shaw GD, Kriz R, Kelleher KS. Identification of peptide antagonists to glycoprotein ibalpha that selectively inhibit von Willebrand factor dependent platelet aggregation. *Biochemistry*. 2008;47:4674–4682. DOI: 10.1021/bi702428q.

22. Chadderdon SM, Belcik JT, Bader L, Kirigiti MA, Peters DM, Kievit P, Grove KL, Lindner JR. Proinflammatory endothelial activation detected by molecular imaging in obese nonhuman primates coincides with onset of insulin resistance and progressively increases with duration of insulin resistance. *Circulation*. 2014;129:471–478. DOI: 10.1161/CIRCULATIONAHA.113.003645.

23. Chung DW, Chen J, Ling M, Fu X, Blevins T, Parsons S, Le J, Harris J, Martin TR, Konkle BA, et al. High-density lipoprotein modulates thrombosis by preventing von Willebrand factor self-association and subsequent platelet adhesion. *Blood*. 2016;127:637–645. DOI: 10.1182/blood-2014-09-599530.

24. Fu X, Cate SA, Dominguez M, Osborn W, Ozpolat T, Konkle BA, Chen J, Lopez JA. Cysteine disulfides (Cys-ss-X) as sensitive plasma biomarkers of oxidative stress. *Sci Rep*. 2019;9:115. DOI: 10.1038/s41598-018-35566-2.

25. Gawaz M, Langer H, May AE. Platelets in inflammation and atherogenesis. *J Clin Invest*. 2005;115:3378–3384. DOI: 10.1172/JCI27196.

26. Chadderdon SM, Belcik JT, Bader L, Peters DM, Kievit P, Alkayed NJ, Kaul S, Grove KL, Lindner JR. Temporal changes in skeletal muscle capillary responses and endothelial-derived vasodilators in obesity-related insulin resistance. *Diabetes*. 2016;65:2249–2257. DOI: 10.2337/db15-1574.

27. Rurali E, Noris M, Chianca A, Donadelli R, Banterla F, Galbusera M, Gherardi G, Gastoldi S, Parvanova A, Iliev I, et al. ADAMTS13 predicts renal and cardiovascular events in type 2 diabetic patients and response to therapy. *Diabetes*. 2013;62:3599–3609. DOI: 10.2337/db13-0530.

28. Meigs JB, O'Donnell CJ, Tofler GH, Benjamin EJ, Fox CS, Lipinska I, Nathan DM, Sullivan LM, D'Agostino RB, Wilson PW. Hemostatic markers of endothelial dysfunction and risk of incident type 2 diabetes: the Framingham offspring study. *Diabetes*. 2006;55:530–537. DOI: 10.2337/diabetes.55.02.06.db05-1041.

29. Seligman BG, Biolo A, Polanczyk CA, Gross JL, Clausell N. Increased plasma levels of endothelin 1 and von Willebrand factor in patients with type 2 diabetes and dyslipidemia. *Diabetes Care*. 2000;23:1395–1400. DOI: 10.2337/diacare.23.9.1395.

30. Jimenez MA, Novelli E, Shaw GD, Sundd P. Glycoprotein ibalpha inhibitor (CCP-224) prevents neutrophil-platelet aggregation in sickle cell disease. *Blood Adv*. 2017;1:1712–1716. DOI: 10.1182/bloodadvances.2017006742.

31. Ozawa K, Muller MA, Varlamov O, Tavori H, Packwood W, Mueller PA, Xie A, Ruggeri Z, Chung D, Lopez JA, et al. Proteolysis of von willebrand factor influences endothelial activation and vascular compliance in atherosclerosis. *JACC Basic Transl Sci*. 2020;5:1017–1028. DOI: 10.1016/j.jacbts.2020.08.009.

32. Taye A, Saad AH, Kumar AH, Morawietz H. Effect of apocynin on NADPH oxidase-mediated oxidative stress-LOX-1-eNOS pathway in human endothelial cells exposed to high glucose. *Eur J Pharmacol*. 2010;627:42–48. DOI: 10.1016/j.ejphar.2009.10.045.

33. Barry-Lane PA, Patterson C, van der Merwe M, Hu Z, Holland SM, Yeh ET, Runge MS. p47phox is required for atherosclerotic lesion progression in ApoE(-/-) mice. *J Clin Invest*. 2001;108:1513–1522. DOI: 10.1172/JCI200111927.

34. Oggianu L, Lancellotti S, Pitocco D, Zaccardi F, Rizzo P, Martini F, Ghirlanda G, De Cristofaro R. The oxidative modification of von Willebrand

factor is associated with thrombotic angiopathies in diabetes mellitus. *PLoS One*. 2013;8:e55396. DOI: 10.1371/journal.pone.0055396.

35. Samocha-Bonet D, Justo D, Rogowski O, Saar N, Abu-Abeid S, Shenkerman G, Shapira I, Berliner S, Tomer A. Platelet counts and platelet activation markers in obese subjects. *Mediators Inflamm*. 2008;2008:1–6. DOI: 10.1155/2008/834153.

36. Wu JJ, Fujikawa K, Lian EC, McMullen BA, Kulman JD, Chung DW. A rapid enzyme-linked assay for ADAMTS-13. *J Thromb Haemost*. 2006;4:129–136. DOI: 10.1111/j.1538-7836.2005.01677.x.

37. Varadi K, Rottensteiner H, Vejda S, Weber A, Muchitsch EM, Turecek PL, Ehrlich HJ, Scheiflinger F, Schwarz HP. Species-dependent variability of ADAMTS13-mediated proteolysis of human recombinant

von Willebrand factor. *J Thromb Haemost*. 2009;7:1134–1142. DOI: 10.1111/j.1538-7836.2009.03453.x.

38. Muia J, Zhu J, Greco SC, Vanhoorelbeke K, Gupta G, Westfield LA, Sadler JE. Phylogenetic and functional analysis of ADAMTS13 identifies highly conserved domains essential for allosteric regulation. *Blood*. 2019;133:1899–1908. DOI: 10.1182/blood-2018-11-886275.

39. Turner NA, Moake JL, Kamat SG, Schafer AI, Kleiman NS, Jordan R, McIntire LV. Comparative real-time effects on platelet adhesion and aggregation under flowing conditions of in vivo aspirin, heparin, and monoclonal antibody fragment against glycoprotein IIb-IIIa. *Circulation*. 1995;91:1354–1362. DOI: 10.1161/01.CIR.91.5.1354.

SUPPLEMENTAL MATERIAL

Data S1.

Supplemental Methods

Flow cytometry

Platelet-rich plasma was immediately isolated from whole blood collected into sodium citrate tubes and was stored at -80° C. Thawed samples were used for platelet staining with anti-human antibodies known to cross react with non-human primates at dilutions determined by appropriate titration experiments. Platelet were stained using FITC-labeled anti-human CD41 monoclonal antibody (HIP8; BioLegend, San Diego, CA) at 1:200 dilution. Staining for p-selectin was performed using a biotinylated p-selectin glycoprotein ligand-1 dimeric fusion protein with human immunoglobulin-1 (YSPSL) which cross reacts with the macaque species. Secondary staining was performed with FITC-labeled streptavidin (BD Biosciences). Control experiments with isotype control antibody and no antibody were performed to establish 99.9% exclusion gates. Flow-cytometry analysis was performed using a FACSCanto II (BD Biosciences). Forward-scatter area and side-scatter area profiles together with presence of any CD41 staining were used to gate for the platelet population. Data were expressed as the geometric mean fluorescence intensity for events beyond the 99.9% exclusion gate. Experiments were performed in duplicate.

LC-MS/MS Analysis

Aliquots of whole blood and plasma were snap frozen and stored at -80° C until analysis. Plasma protein concentration was measured by the Bradford assay (Bio-Rad, Hercules, CA) using bovine serum albumin as the standard. To measure small molecular thiols and disulfides, samples

were mixed 1:1 with 5 mM N-ethylmaleimide in 5 mM PBS, pH 6.0, for 30 minutes at 37° C. For

total thiols and disulfides, 20 μL samples were reduced with 80 μL of 12 mM dithiothreitol in 20

mM PBS, pH 7.4, for 20 min at 65° C. Samples were then alkylated with 40 mL of 60 mM N-

ethylmaleimide in 5 mM PBS, pH 6.5, for 20 minutes at 65° C. Protein precipitation was performed

with methanol (80% final v/v/) for 1 hour at -20° C followed by centrifugation at 20,000 g for 20

min. The supernatant was diluted (10% v/v) in 0.01% acetic acid. LC-MS/MS analysis was

performed using a Waters ACQUITY I-Class ultra-performance liquid chromatograph coupled to

a SCIEX QTRAP 6500 mass spectrometer with standard electrospray ionization source. Analytes

were separated using a Waters HSS T3 column at 40° C. Analysis was performed as described in

on-line Supplemental Methods, and whole blood samples were normalized to hemoglobin

concentration while plasma samples were normalized to total protein.

Mobile phase A was 0.1% formic acid in water and mobile phase B was 0.1% formic acid

in acetonitrile. Samples (5 or 10 μl) were injected using an autosampler at 8 °C. Analytes were

eluted at a flow rate of 0.3 ml/min with a gradient of increasing mobile phase B concentration, as

follows: 0.2% for 1 min, 0.2% to 10% for 1 min, 10% to 25% for 4 min, and 25% to 90% for 2

min. The column was cleaned with 90% mobile phase B for 1.5 min and then equilibrated with

0.2% mobile phase B for 5 min. Analytes were detected in the mass spectrometer using MRM in

positive mode under the following conditions: ion spray voltage: 5500 V, temperature: 550 °C,

curtain gas: 40 psi, collision gas: high, ion source gas 1: 45 psi, ion source gas 2: 50 psi, entrance

potential: 10 V, collision cell exit potential: 11 V. The detailed conditions for MRM transitions,

optimized declustering potential (DP), and collision energy (CE) are listed in Table 1. All LC-

MS/MS systems were controlled by Analyst® software version 1.6.2 (SCIEX) and MRM data

were acquired using the same software. LC-MS/MS-MRM data was processed using MultiQuant

2.1 software (SCIEX). The peak area was used to quantify the concentration of analytes as follows:

A. If the isotopically labeled analyte was present in the internal standard, the concentration of the

corresponding analyte in samples was calculated by:

$$[a] = \frac{(Peak\ area)_{a^*}}{(Peak\ area)_{a^*}} \times [a^*]$$

where a^* is the isotopically labeled analyte in the internal standard with known concentration, and

a is the corresponding analyte. The concentration of protein-bound thiols was considered to be

equal to the concentration of total thiols an disulfides minus the concentration of total small

molecular thiols and disulfides.

Table S1. Vital Signs at the Time of Vascular Assessment Under Basal Conditions and During Adenosine Stress*.

		Obese		
	Lean (n=6)	Baseline	8 Wks Apocynin	p-value
Baseline				
Heart rate (bpm)	136 (119-144)	128 (117-136)	105 (100-137)	0.14
Systolic BP (mm Hg)	82 (70-104)	84 (73-96)	72 (56-88)	0.72
Diastolic BP (mm Hg)	44 (35-50)	43 (34-63)	35 (27-44)	0.40
Adenosine				
Heart rate (bpm)	138 (117-149)	144 (132-145)	137 (131-141)	0.68
Systolic BP (mm Hg)	85 (74-99)	95 (75-103)	95 (66-114)	0.87
Diastolic BP (mm Hg)	38 (33-48)	45 (37-54)	46 (35-71)	0.53

*Data are display as median (interquartile range); p-values were calculated by Kruskal-Wallis test.

Figure S1. (A) Thiol composition in whole blood measured by mass spectrometry. Data from 11 animals (lean: n=6, WSD: n=5) are displayed. (B) Protein-bound thiol composition in plasma measured by mass spectrometry.
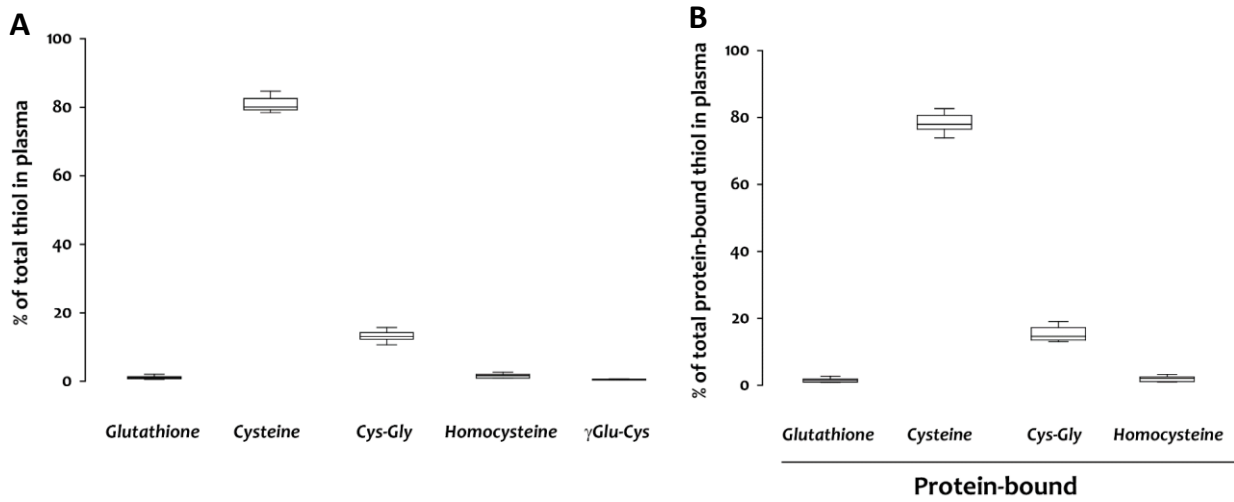
Data from 11 animals (lean: n=6, WSD: n=5) are displayed.

Figure S2. Correlation between common carotid average IMT and CEU-derived molecular imaging signal for GPIbα or VCAM-1.
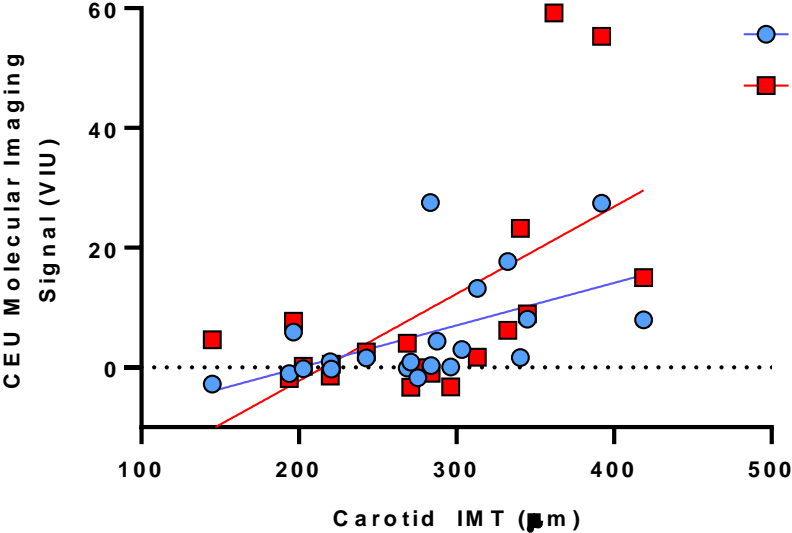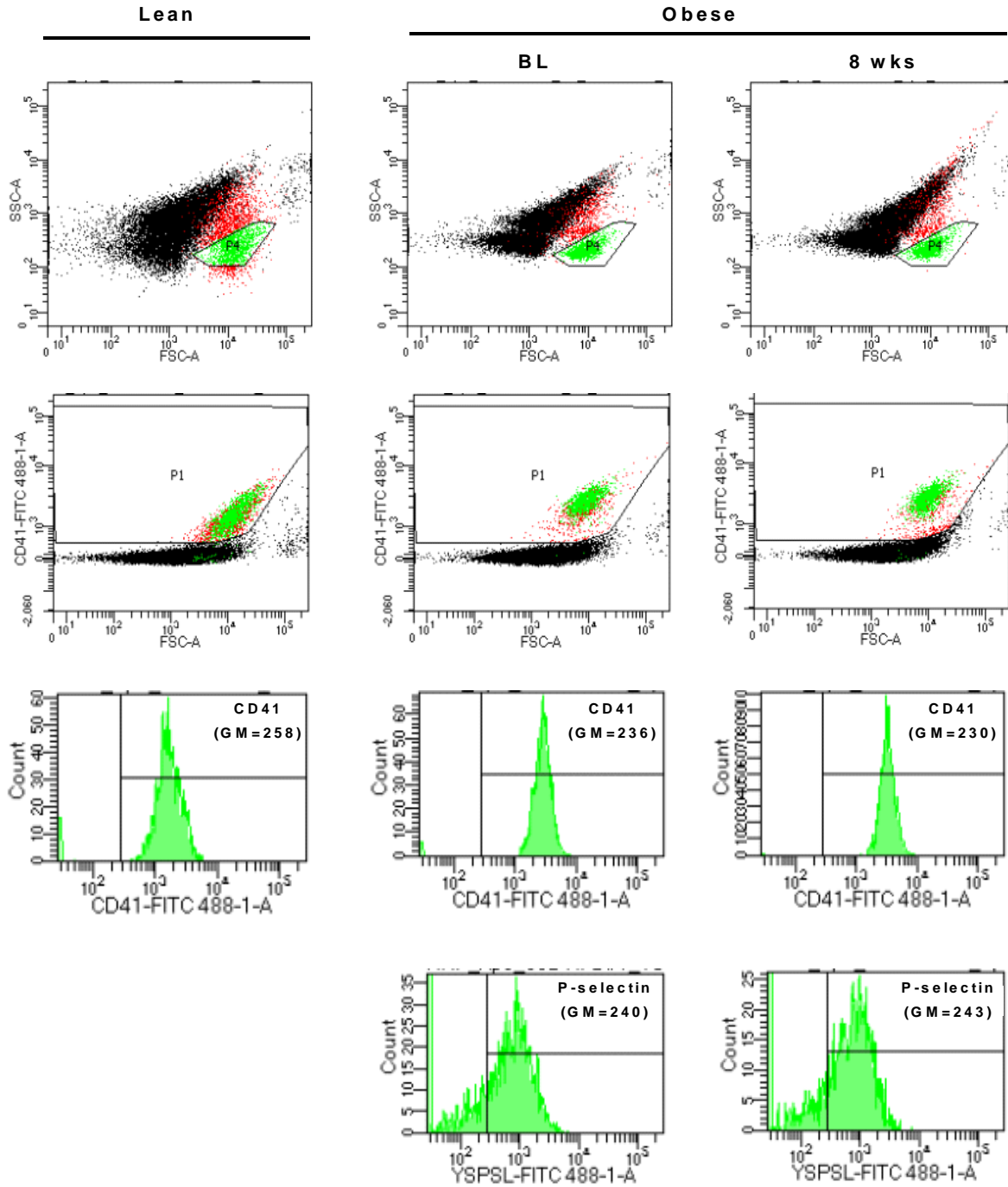
Figure S3. Examples of flow cytometry data for platelet activation status.

A combination of side versus forward light scatter (top rows) and positive staining for any CD41 (second row) were used to identify the platelet population (indicated by green events). Histograms for fluorescent intensity on staining for CD41 (third row) and p-selectin (bottom row) are shown. Geometric means (*GM*) are provided for events beyond the 99.9% exclusion gate from control experiments, illustrated by events to the right of the vertical line.